The Aeronautical Journal (2025), **129**, pp. 432–456
doi:10.1017/aer.2024.98

ROYAL AERONAUTICAL SOCIETY

RESEARCH ARTICLE

Nonlinear unsteady behaviour study for jet transport aircraft response to serious atmosphere turbulence

W. Jiang, H. Guo, Z. Li and R.C. Chang

Flight College, Changzhou Institute of Technology, Changzhou, Jiangsu, China
Corresponding author: R. Chang; Email: zangrc@czu.cn

Received: 9 November 2023; **Revised:** 30 June 2024; **Accepted:** 16 July 2024

Keywords: atmosphere turbulence; fuzzy-logic modeling (FLM); aerodynamics model; flight environment; oscillatory motion; controllability

Abstract

The main purpose of this article is to present the nonlinear unsteady behaviour for jet transport aircraft response to serious atmosphere turbulence in cruise flight and to provide the appropriate mitigation concepts for pilots in the pilot training course of the IATA – Loss of Control In-flight (LOC-I) program. The flight data of a twin-jet and a four-jet transport aircraft encountered serious atmosphere turbulence are the study cases for this article. This study uses flight data mining and fuzzy-logic modeling of artificial intelligence techniques to establish nonlinear unsteady aerodynamic models. Since the rapid change of aerodynamic characteristics in turbulence, so the study uses decoupled longitudinal and lateral-directional motion to identify various eigenvalue motion modes of nonlinear unsteady behaviour through digital 6-DOF flight simulation. It is found that the changes of the main flight variables in the aerodynamic scene and flight environment of the two aircraft are different, but the profiles of five eigenvalue motion modes are actually similar. Those similar eigenvalue motion modes can formulate preventive actions related to the flight handling quality for safe and efficient control by pilots to execute the flight tasks. The one with a large drop height during the ups and downs motion between the two is chosen to construct the movement mechanism of nonlinear unsteady behaviours. The assessments of dynamic stability characteristics of nonlinear unsteady behaviour based on the approaches of oscillatory motion and eigenvalue motion modes related to loss of control will be demonstrated in this article. To develop preventive actions, the situation awareness response to the induced mutation of nonlinear unsteady behaviour on the pilot's operations will be a further research task in the future.

Nomenclature

$A(x_r)$	membership function for input variable x_1
$\bar{A}_1$	I_{xz}/I_{xx} products of inertia/moments of inertia about x-axes
a_z	normal accelerations (g)
b	wing span (m)
$\bar{B}_1$	I_{xz}/I_{zz} products of inertia/moments of inertia about z-axes
C_x, C_z, C_m	longitudinal aerodynamic force and moment coefficients
C_y, C_l, C_n	lateral-directional aerodynamic force and moment coefficients
$\bar{c}$	mean aerodynamic chord (m)
g	gravity acceleration (m/s^2)
h	altitude (m)
I_{xx}, I_{yy}, I_{zz}	moments of inertia about x-, y-, and z-axes, respectively (kg·m^2)
I_{xy}, I_{xz}, I_{yz}	products of inertia (kg·m^2)
k_1, k_2	longitudinal and lateral-directional reduced frequencies, respectively
L, M, N	moments acting about the (x,y,z)-body axes of aircraft, respectively (N·m)
M	Mach number

m	aircraft mass (kg)
p, q, r	body-axis roll rate, pitch rate and yaw rate (deg./s.)
$\bar{q}$	dynamic pressure (kpa)
R^2	square of multiple correlation coefficients
S	wing reference area (m^2)
T_x	thrust term along the x-body axis of the aircraft (N)
T_m	thrust-moment term in the pitching equation of motion (N)
t	time (sec)
T, W	thrust and aircraft weight in flight, N, respectively
X, Y, Z	forces acting on the aircraft body-fixed axes along x-, y- and z-axes, N, respectively
$\alpha, \dot{\alpha}$	angle-of-attack, deg. and time rate of change of angle-of-attack, deg./sec., respectively
$\beta, \dot{\beta}$	sideslip angle, deg. and time rate of change of sideslip angle, deg./sec., respectively
$\delta_a, \delta_e, \delta_r$	control deflection angles of aileron, elevator and rudder, respectively (deg.)
ϕ, θ, ψ	Euler angles in roll, pitch and yaw, respectively (deg.)
λ_r, λ_i	eigenvalue in real (i.e. in-phase) and imaginary (i.e. out-of-phase) parts, respectively
ζ	damping ratio
ωn	natural frequency

Abbreviation

FDR	flight data recorder
FLM	fuzzy-logic modeling
IATA	International Air Transport Association
LOC-I	loss of control in-flight
RMS	root-mean-square

1.0 Introduction

The transport aircraft in flight is subjected serious atmosphere turbulence resulting with the abrupt change in attitude and gravitational acceleration (i.e. the normal load factor) [1]. These varying characteristics not only pose threats to flight safety, but also may cause structural damages and reduce fatigue life [2]. The movement mechanisms [3] of transport aircraft response to serious atmosphere turbulence were studied for the purpose to obtain the loss of control prevention. To formulate preventive actions, the situation awareness of varying crosswind encountering for the operational pilot in the reference of movement mechanisms would be the further study task in the future. A concept of the control strategy in prevention programme [4] was presented to prevent the injuries of passengers and crew members for transport aircraft in serious atmosphere turbulence for the airlines. The constructions of situation awareness and expert strategy knowledge bases required more study cases; these parts would be the future tasks in their research team.

In general, aircraft stability depicts whether the motion will diverge when the aircraft encounters the disturbance from its equilibrium state. The flight handling quality describes whether it's easy for pilot to accomplish the assigned task at different flight phases. This criterion is important for aircraft pilots to verify that the aircraft is controllable without huge workload for a pilot. Research on flight handling quality has been carried out since the aircraft successfully achieved the manned mission. After decades of flight experiments and research, with the increase of flight speed and altitude and the increasing complexity of the operating system, the content of flight handling quality has been continuously expanded to adapt to new situations [5]. In the present, the aerodynamic characteristics of the aircraft and the relationship between the characteristics of the flight dynamics are emphasised. The longitudinal characteristic equations have short-period mode and phugoid mode (long period mode); the lateral-directional characteristic equations have Dutch-roll mode, spiral mode and roll mode.

From the perspective of aircraft characteristics, flight handling quality mainly refers to the stability and manoeuverability of the aircraft. Stability includes static stability and dynamic stability (damping

https://doi.org/10.1017/aer.2024.98 Published online by Cambridge University Press

and frequency values of each disturbance motion mode). Manoeuverability includes control effectiveness, for example, the control of the elevator should maintain the balance of the longitudinal moment of the aircraft; the control of the rudder should maintain the balance of the horizontal yaw moment; and the driving force, the pilot must apply to the control in order to maintain a balanced state or perform a manoeuvering flight. Therefore, the flight handling quality is usually evaluated through simulated flight.

For the past 10 years, International Air Transport Association (IATA) had consistently identified loss of control in flight (LOC-I) as the most significant cause of fatal accidents [6]. LOC-I usually occurs when the aircraft enters a flight condition outside its normal envelope, thereby causing surprise to the crew involved. IATA has made a lot of contributions in recent years in arranging international training courses for pilots. The concept of possible mitigation for loss of control prevention is the most important training course in IATA – Loss of Control in Flight (LOC-I) programme.

To prevent loss of control in flight motions for the pilots and to promote the understanding of nonlinear unsteady behaviour, a new study is conducted in this article to examine the response to serious atmospheric turbulence on the flight manoeuver. The flight data of a twin-jet (Aircraft A) and a four-jet (Aircraft B) transport aircraft encountered serious atmosphere turbulence is the study cases for this article. The weight and size of Aircraft B are larger than those of Aircraft A. The main purpose is to prove that this method can be adapted to aircraft of different weights and sizes through reliability assessment. The flight data mining and fuzzy-logic modeling of artificial intelligence techniques are used to establish nonlinear unsteady aerodynamic models with six aerodynamic coefficients. The service age of Aircraft A is 15 years and 3 months; Aircraft B is 8 years. This article uses decoupled longitudinal and lateral-directional motion to solve the rapid changing problems of aerodynamic forces and moments in turbulence. The eigenvalues of motion are estimated based on damping ratio and undamped natural frequency [7]. A positive real part of the eigenvalues is to indicate unstable motion of the related modes. It is found that the profiles of five eigenvalue motion modes for two aircraft are actually similar; the eigenvalues for phugoid (long-period) and roll modes of motion are stable; the others are unstable.

The one with a large drop height during the ups and downs motion between the two is chosen to construct the movement mechanism of nonlinear unsteady behaviours. Those similar eigenvalue motion modes formulated the preventive actions related to the flight handling quality will be demonstrated in this article. The situation awareness response to the induced mutation of nonlinear unsteady behaviour on the pilot's operations to avoid loss of control can be the training course of the IATA – Loss of Control In-flight (LOC-I) programme.

2.0 Numerical method and modelling

The present study is based on artificial intelligence techniques. The input data of fuzzy-logic modeling (FLM) picks up a specified segment from flight data recorder (FDR), which contains many parameters, but some are not relevant to the research topic of nonlinear unsteady behaviour study. The process of organising this data, filtering out irrelevant data to fit requirements, and then applying it to practical problems is called data mining [8]. The artificial intelligence techniques include two parts: the nonlinear unsteady aerodynamic database development and the aviation accident root cause assessments.

2.1 Aerodynamic database development

Aerodynamic database development includes data manipulation, compatibility check, input information of aircraft main geometry and moment of inertia data, equations of motion, and unsteady thrust model. The flowchart for development is presented in Fig. 1. In references of Chang et al. [9] & Jiang et al. [10] have detail descriptions of data manipulation, compatibility check, equations of motion, and unsteady thrust model.

https://doi.org/10.1017/aer.2024.98 Published online by Cambridge University Press

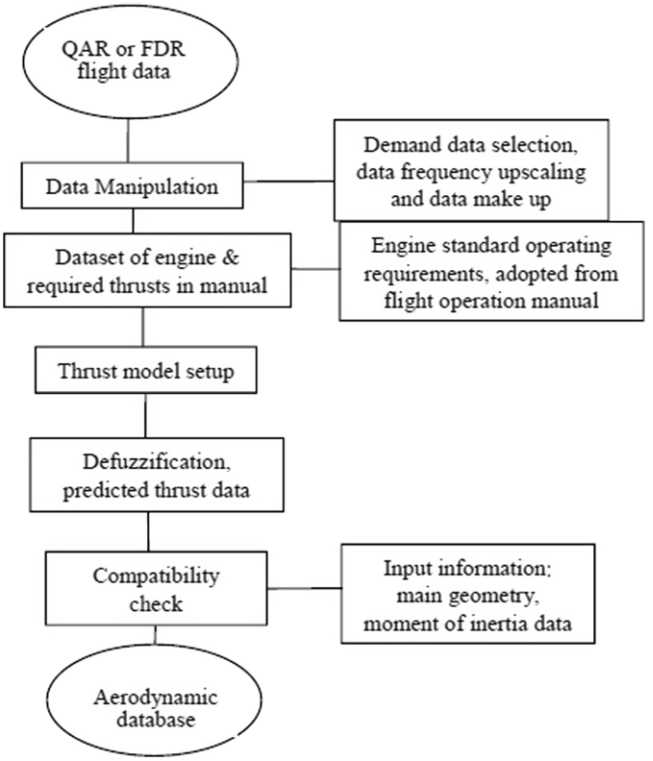

Figure 1. *Flowchart of aerodynamic database development.*

2.2 Development of root caused analysis in aviation accident

This section describes the development of root caused analysis in aviation accident, as shown in Fig. 2. The flowchart of Fig. 2 is based on the data of the nonlinear unsteady aerodynamic database. The fuzzy-logic modeling technique(11,12) is used to setup aerodynamic models. The aerodynamic models can provide the stability and controllability derivatives to be used for the accident analyses. The derivative indices can help to pinpoint the major cause more efficiently while proceeding event or accident investigation to judge about how difficult it was for the pilot or the autopilot system to control the aircraft in loss of control conditions.

2.3 Nonlinear unsteady aerodynamic models

For unsteady aerodynamic modeling, in the late 2009, two preferred modeling methods emerged based on neural network [7] and fuzzy-logic algorithm [13]. For the aerodynamic modeling using fuzzy-logic algorithm, the accuracy of modeling is adjusted by studying the selection of membership functions. The number of modeling parameters without limit setting is the advantage of this fuzzy-logic modeling method. Modeling means to establish the numerical relationship among certain variables of interest. In the fuzzy-logic model, more complete necessary influencing flight variables can be included to capture all possible effects on aircraft response to specify applications.

The longitudinal main aerodynamics is assumed to depend on the following ten flight variables [3]:

$$C_x, C_z, C_m = f(\alpha, \dot{\alpha}, q, k_1, \beta, \delta_e, M, p, \delta_s, \bar{q}) \tag{1}$$

https://doi.org/10.1017/aer.2024.98 Published online by Cambridge University Press

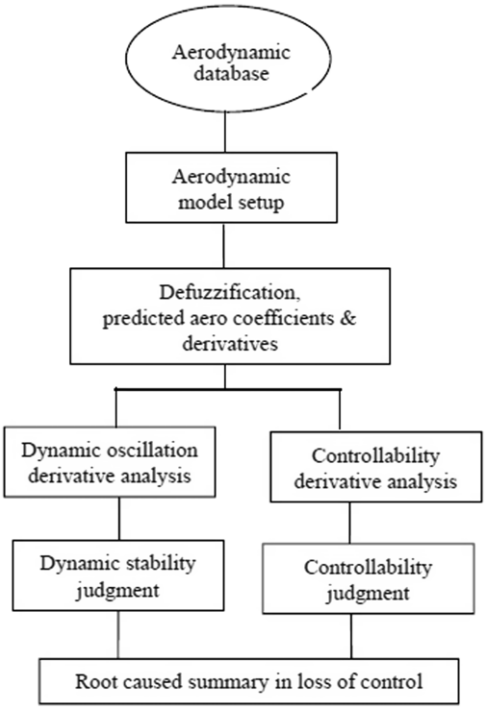

Figure 2. *Flowchart for aviation accident root cause assessment.*

The coefficients on the left-hand side of Equation (1) represent the coefficients of axial force (C_x), normal force (C_z), and pitching moment (C_m), respectively. The variables on the right-hand side of Equation (1) are defined as follows: angle-of-attack (α), time rate of angle-of-attack ($d\alpha/dt$, or $\dot{\alpha}$), pitch rate (q), longitudinal reduced frequency (k_1), sideslip angle (β), control deflection angle of elevator (δ_e), Mach number (M), roll rate (p), stabiliser angle (δ_s), and dynamic pressure ($\bar{q}$). These variables are called the influencing variables. The roll rate is included here because it is known that an aircraft encountering hazardous weather tend to develop rolling which may affect longitudinal stability. The variable of dynamic pressure is for estimation of the significance in structural deformation effects.

For the lateral-directional aerodynamics to depend on the following 11 flight variables [3],

$$C_y, C_l, C_n = f(\alpha, \beta, \phi, p, r, k_2, \delta_a, \delta_r, M, \dot{\alpha}, \beta \tag{2}$$

The coefficients on the left-hand side of Equation (2) represent the coefficients of side force (C_y), rolling moment (C_l) and yawing moment (C_n), respectively. The variables on the righthand side of Equation (2) are defined as follows: angle-of-attack (α), sideslip angle (β), roll angle (ϕ), roll rate (p), yaw rate (r), lateral-directional reduced frequency (k_2), control deflection angle of aileron (δ_a), control deflection angle of rudder (δ_r), Mach number (M), the time rate of angle-of-attack ($\dot{\alpha}$), and the time rate of sideslip angle ($\dot{\beta}$).

2.4 Model-based derivatives

The basic definition of a derivative is that the tangent slope of a point on a curve is the derivative of that point. In this study, the difference-in-center method is used to calculate the derivative value, that is, the abscissa value at the point, and add and subtract a minor abscissa value of the same value, which corresponds to the slope of the line connecting the two points on the curve. Fuzzy-logic modeling is very important in the aerodynamic performance analysis of real flight data. The effectiveness criteria

https://doi.org/10.1017/aer.2024.98 Published online by Cambridge University Press

Table 1. *The effectiveness criteria for derivative values of stability, damping, and controllability [3]*

Orientation	Sort	Derivative	Units	Derivative Description	Effectiveness
Longitudinal	Static Stability	$C_{z\alpha}$	rad^{-1}	Derivative of C_z with respect to α	+
		$C_{m\alpha}$	rad^{-1}	Derivative of C_m with respect to α	–
	Dynamic stability	$C_{z\dot{\alpha}}$	rad^{-1}	Derivative of C_z with respect to $\dot{\alpha}$	+
		$C_{m\dot{\alpha}}$	rad^{-1}	Derivative of C_m with respect to $\dot{\alpha}$	–
	Damping	C_{zq}	rad^{-1}	Derivative of C_z with respect to q	+
		C_{mq}	rad^{-1}	Derivative of C_m with respect to q	–
	Controllability	$C_{m\delta e}$	rad^{-1}	Derivative of C_m with respect to δ_e	–
Lateral & directional	Static stability	$C_{l\beta}$	rad^{-1}	Derivative of C_l with respect to β	–
		$C_{n\beta}$	rad^{-1}	Derivative of C_n with respect to β	+
	Dynamic stability	$C_{l\dot{\beta}}$	rad^{-1}	Derivative of C_l with respect to $\dot{\beta}$	–
		$C_{n\dot{\beta}}$	rad^{-1}	Derivative of C_n with respect to $\dot{\beta}$	+
	Damping	C_{lp}	rad^{-1}	Derivative of C_l with respect to p	–
		C_{nr}	rad^{-1}	Derivative of C_n with respect to r	–
	Controllability	$C_{n\delta r}$	rad^{-1}	Derivative of C_n with respect to δ_r	–
		$C_{l\delta a}$	rad^{-1}	Derivative of C_l with respect to δ_a	+

Remarks: The effectiveness is judged based on the positive or negative of derivative value.

for derivative values of stability, damping and controllability are shown in Table 1. The root caused analysis for aircraft accident due to the pilots in loss of control are based on the assessment of those derivatives [3].

2.5 Flight simulation of flight handling quality

The guidelines of flying quality in civil airplane are expressed in damping ratios and natural frequencies, The time to double or halve the amplitude of initial disturbances is described in Ref. [10], defined as:

$$T_2 = \frac{\ln 2}{-\varsigma\omega_n} \tag{3}$$

where ζ is the damping ratio and ω_n is the natural frequency. Note that -ζω_n is the real part of the eigenvalues. If it is positive, the system is unstable and T_2 is also positive, representing the time to double the amplitude. On the other hand, if it is negative, the system is stable, and T_2 is negative, representing the time to halve the amplitude. In this latter case, T_2 is replaced by $T_{1/2}$ and '2' in Equation (3) is replaced by $^1/_2$. For simplicity in the computer output, T_2 will be used in all cases, with the understanding that if it is negative, it should be the time to halve the amplitude.

From the above considerations, the first step in evaluating the flying qualities is to determine the eigenvalues of an airplane along the flight trajectory. In the present approach, one will numerically integrate the 6-DOF dynamic equations of motion to determine the eigen-modes of motion at the same time at every instant. The matrix for the eigenvalues consists of the first derivatives evaluated at the instant under consideration, not about the trim points as done conventionally. Note that in abnormal flight conditions there may not be trim points.

It is easier to extract the stability characteristics by formulating the equations in the stability axes. Therefore, in the present study of flight simulation, the general equations of motion in the following are integrated:

https://doi.org/10.1017/aer.2024.98 Published online by Cambridge University Press

$$\frac{d\alpha}{dt} = f_1 = \left\{\left[\left(-\frac{X}{m} + g\sin\theta\right)/V - r\sin\beta\right]\sin\alpha + \left[\left(\frac{Z}{m} + g\cos\theta\cos\varphi\right)/V - p\sin\beta\right]\cos\alpha\right\} / \cos\beta + q \tag{4}$$

$$\frac{d\beta}{dt} = f_2 = \left[-\left(\frac{X}{m} - g\sin\theta\right)\sin\beta/V - r\right]\cos\alpha + \left(\frac{Y}{m} + g\cos\theta\sin\varphi\right)\cos\beta/V \left[-\left(\frac{Z}{m} + g\cos\theta\cos\varphi\right)\sin\beta/V + p\right]\sin\alpha \tag{5}$$

$$\frac{dp}{dt} = f_3 = \left[L + \frac{I_{xz}N}{I_{zz}} + I_{xz}\left(1 + \frac{I_{xx} - I_{yy}}{I_{zz}}\right)pq + \left(I_{yy} - I_{zz} - \frac{I_{xz}^2}{I_{zz}}\right)qr\right]/(AI_{xx}) \tag{6}$$

$$\frac{dq}{dt} = f_4 = [M + I_{xz}(r^2 - p^2) + (I_{zz} - I_{xx})rp]/I_{yy} \tag{7}$$

$$\frac{dr}{dt} = f_5 = \left[\frac{I_{xz}L}{I_{xx}} + N + \left(I_{xx} - I_{yy} + \frac{I_{xz}^2}{I_{xx}}\right)pq + \left(\frac{I_{yy} - I_{zz}}{I_{xx}} - 1\right)I_{xz}qr\right]/(AI_{zz}) \tag{8}$$

$$\frac{d\theta}{dt} = f_6 = q\cos\varphi - r\sin\varphi \tag{9}$$

$$\frac{d\varphi}{dt} = f_7 = p + \tan\theta(q\sin\varphi + r\cos\varphi) \tag{10}$$

$$\frac{dV}{dt} = f_8 = \left(\frac{X}{m} - g\sin\theta\right)\cos\alpha\cos\beta + \left(\frac{Y}{m} + g\cos\theta\sin\varphi\right)\sin\beta + \left(\frac{Z}{m} + g\cos\theta\cos\varphi\right)\sin\alpha\cos\beta \tag{11}$$

where $A = 1 - \frac{I_{xz}^2}{I_{xx}I_{zz}}$, and *X, Y, Z, L, M, N* are the forces and moments acting on the transport and are estimated from the fuzzy-logic aerodynamic models.

To determine the flying qualities, one needs the eigenvalues of the linearised equations. Instead of using an 'average' linearised system, linearisation is done at every time instant, i.e. the so-called time linearisation, as indicated earlier. In other words, a system of matrix (A) consisting of $\partial f_i/\partial x_j$, $i = 1,\ldots,8$ and $j = 1,\ldots,8$, is determined while the time integration of the dynamic equation is performed, where x_j stands for α, β, p, q, r, θ, ϕ and V, respectively, for $j = 1, \ldots, 8$. Note that the inertial effects from the moments of inertia are incorporated. The inertial effects could become essential in recovering a flight vehicle from stall, or when the conventional control surfaces are not effective. To determine the eigenvalues of A, the QR transformation technique is employed. Unfortunately, it is difficult to identify the individual modes of motion from these eigenvalues from one instant to another because of the rapid changes of aerodynamic forces and moments in turbulence. One approach to solve this problem is to use the approximate modes of motion obtained from decoupled longitudinal and lateral-directional Equations (14) as guidance.

(1) The decoupled linearised longitudinal equations of motion are as follows:

$$\dot{u} = -g\theta\cos\theta_1 + X_u u + X_\alpha\alpha + X_{\delta e}\delta e \tag{12}$$

$$U_1\dot{\alpha} - U_1\dot{\theta} = -g\theta\sin\theta_1 + Z_u u + Z_\alpha\alpha + Z_{\dot{\alpha}}\dot{\alpha} + Z_q\dot{\theta} + Z_{\delta e}\delta e \tag{13}$$

$$\ddot{\theta} = M_u u + M_\alpha\alpha + M_{\dot{\alpha}}\dot{\alpha} + M_q\dot{\theta} + M_{\delta e}\delta e \tag{14}$$

https://doi.org/10.1017/aer.2024.98 Published online by Cambridge University Press

where the $\dot{u}$is accelerations in X axis direction; U_1 is disturbance introduced speed in X axis direction of atmosphere turbulence; θ and θ_1 are pitch angle and disturbance introduced pitch angle in atmosphere turbulence, respectively; X_u, X_α, and $X_{\delta e}$are the dimensional alteration of force along X axis with the speed, angle-of-attack, and elevator angle, respectively; Z_u, Z_α, $Z_{\dot{\alpha}}$, Z_q, and $Z_{\delta e}$ are the dimensional alteration of force along Z axis with the speed, angle-of-attack, time rate of angle-of-attack, pitch rate and elevator angle, respectively. M_u, M_α, $M_{\dot{\alpha}}$, M_q, and $M_{\delta e}$ are the dimensional alteration of moment about Y axis with the speed, angle-of-attack, time rate of angle-of-attack, pitch rate and elevator angle.

(2) The decoupled lateral-directional equations of motion are:

$$U_1\dot{\beta} + U_1\dot{\psi} = g\varphi\cos\theta_1 + Y_\beta\beta + Y_p\dot{\varphi} + Y_r\dot{\psi} + Y_{\delta a}\delta a + Y_{\delta r}\delta r \tag{15}$$

$$\ddot{\varphi} - \bar{A}_1\ddot{\psi} = L_\beta\beta + L_p\dot{\varphi} + L_r\dot{\psi} + L_{\delta a}\delta a + L_{\delta r}\delta r \tag{16}$$

$$\ddot{\psi} - \bar{B}_1\ddot{\varphi} = N_\beta\beta + N_p\dot{\varphi} + N_r\dot{\psi} + N_{\delta a}\delta a + N_{\delta r}\delta r \tag{17}$$

where $\bar{A}_1 = I_{xz}/I_{xx}$ and $\bar{B}_1 = I_{xz}/I_{zz}$; Y_β, Y_p, Y_r, $Y_{\delta a}$ and $Y_{\delta r}$ are the dimensional alteration of force along Y axis with the sideslip angle, roll rate, yaw rate, aileron angle and rudder angle, respectively; L_β, L_p, L_r, $L_{\delta a}$, and $L_{\delta r}$ are the dimensional alteration of moment about X axis with the sideslip angle, roll rate, yaw rate, aileron angle and rudder angle, respectively. N_β, N_p, N_r, $N_{\delta a}$, and $N_{\delta r}$ are the dimensional alteration of moment about Z axis with the sideslip angle, roll rate, yaw rate, aileron angle and rudder angle, respectively.

The detail dimensional derivatives of X, Y, Z, M, L and N are described and given in reference of Roskam 2018 [14]. The characteristic equations of Equations (12)–(14) and (15)–(17) are quadratic polynomials. Their roots are solved by the quadratic factorisation method of the Lin-Bairstow algorithm based on the reference of Hovanesian and Pipes 1969 [15].

The 4th degree polynomial of the longitudinal eigen equation has four roots; they are two complex conjugates [7]. The short-period mode is one of the two complex conjugation modes. Another one is phugoid mode (long-period mode). Each pattern has the same real part, but the imaginary part is equal in size and with reverse sign. The 4th degree polynomial of the transverse eigen equation also has four roots; they are a pair of complex conjugations and two real numbers. This pair of composite conjugates represent the Dutch-rolling pattern. One of the two real values represents the spiral mode and another one represents the rolling mode.

3.0 Numerical results and discussions

The aerodynamics and flight characteristics of transport aircraft vary rapidly when subject to serious atmospheric turbulence. These fast change characteristics not only pose threats to flight safety, but also may cause structural damages and reduce fatigue life. To formulate the preventive actions related to the flight handling quality, the study of movement mechanism based on eigenvalues of motion modes would be needed.

3.1 Basic aircraft data required for modeling

The force and moment coefficients in equations of motion require to input the information of main geometry and moment of inertia data [15] for the jet transports. The data of main geometry and moments of inertia for these two transports are presented in Table 2:

The moment (or product) of inertia in Table 2 is estimated by Weight Sizing Module, Advanced Aircraft Analysis (AAA), aircraft design software (DARcorporation 2018) [16]. The Weight Sizing Module allows determination of mission segment fuel fractions and moment (or product) of inertia. Aircraft A and B are symmetrical about the XZ plane; the case it automatically follows that: $I_{xy} = I_{yz} = 0$; both parameters are not shown in Table 2. Both values of I_{xz} in Table 2 are zero due to the clean

https://doi.org/10.1017/aer.2024.98 Published online by Cambridge University Press

Table 2. *Main geometry and moment of inertia data for Aircraft A & B*

Parameter	Aircraft A	Aircraft B
Takeoff gross weight (kg)	145,986	289,524
Wing reference area, S (m^2)	260.0	541.1
Mean chord length,$\bar{c}$ (m)	6.608	7.793
Wing span, b (m)	44.827	64.386
Moment of inertia-*x* axis, I_{xx} ($kg{\cdot}m^2$)	10,710,000	11,300,061
Moment of inertia-*y* axis, I_{yy} ($kg{\cdot}m^2$)	14,883,800	16,591,279
Moment of inertia-*z* axis, I_{zz} ($kg{\cdot}m^2$)	25,283,271	27,552,369
Moment of inertia-xz axes, I_{xz} ($kg{\cdot}m^2$)	0.0	0.0

Table 3. *Final models of longitudinal aerodynamics for Aircraft A*

Coefficient	$\alpha, \dot{\alpha}, q, k_1, \beta, \delta_e, M, p, \delta_s, \bar{q}$	n	R^2
C_z	2 4 2 2 4 2 2 2 3 2	6,912	0.978928
C_m	2 2 4 2 2 4 2 2 2 2	6,144	0.957886

Table 4. *Final models of lateral-directional aerodynamics for Aircraft A*

Coefficient	$\alpha, \beta, \phi, p, r, k_2, \delta_a, \delta_r, M, \dot{\alpha}, \dot{\beta}$	n	R^2
C_l	4 2 2 4 2 2 2 2 2 2 2	13,824	0.953356
C_n	2 2 2 2 4 2 2 4 2 2 2	13,824	0.943465

Table 5. *Final models of longitudinal aerodynamics for Aircraft B*

Coefficient	$\alpha, \dot{\alpha}, q, k_1, \beta, \delta_e, M, p, \delta_s, \bar{q}$	n	R^2
C_z	4 2 2 3 2 2 2 4 2 2	6,912	0.988310
C_m	3 3 3 2 3 2 2 2 2 3	7,776	0.966675

configuration in cruise flight. The value of I_{xz} is not zero, when transport aircraft in takeoff and landing phases with landing gears and high-lift devices as the configuration (Lan and Chang, 2018) [11].

3.2 Analysis of model predictions

Aircraft A and B encountered serious atmosphere turbulence at the altitude around 10,050 m and 11,277 m in transonic flights, respectively. As a result, several passengers and cabin crews sustained injuries, because of which these two events were classified as the aviation accidents. The corresponding flight data of Aircraft A and B are extracted from FDR in time spans $t = 3{,}910$– $3{,}990$s and $t = 6{,}805 \sim 6{,}895$s, respectively.

The aerodynamic coefficient variations of vertical force C_z, pitching moment C_m, rolling moment C_l, and yawing moment C_n are worthy of attention; those aerodynamic coefficients are regarded as main aerodynamic coefficients in the present study.

The final main aerodynamic models of aerodynamic coefficients consist of many fuzzy rules for each coefficient as described from Tables 3–6. In Tables, the numbers below each input variable represents optimum structure in membership function. The total number of fuzzy cells (n) in each model is the product of each number which presented in column 3. The last column shows the final multiple correlation coefficients (R^2). The accuracy of the established aerodynamic model through the fuzzy-logic algorithm can be judged by the multiple correlation coefficients (R^2).

https://doi.org/10.1017/aer.2024.98 Published online by Cambridge University Press

Table 6. *Final models of lateral-directional aerodynamics for Aircraft B*

Coefficient	$\alpha, \beta, \phi, p, r, k_2, \delta_a, \delta_r, M, \dot{\alpha}, \dot{\beta}$	n	R^2
C_l	2 2 2 2 2 2 2 2 2 4 2	13,824	0.972152
C_n	2 4 2 2 2 2 2 2 2 2 4	12,288	0.983331

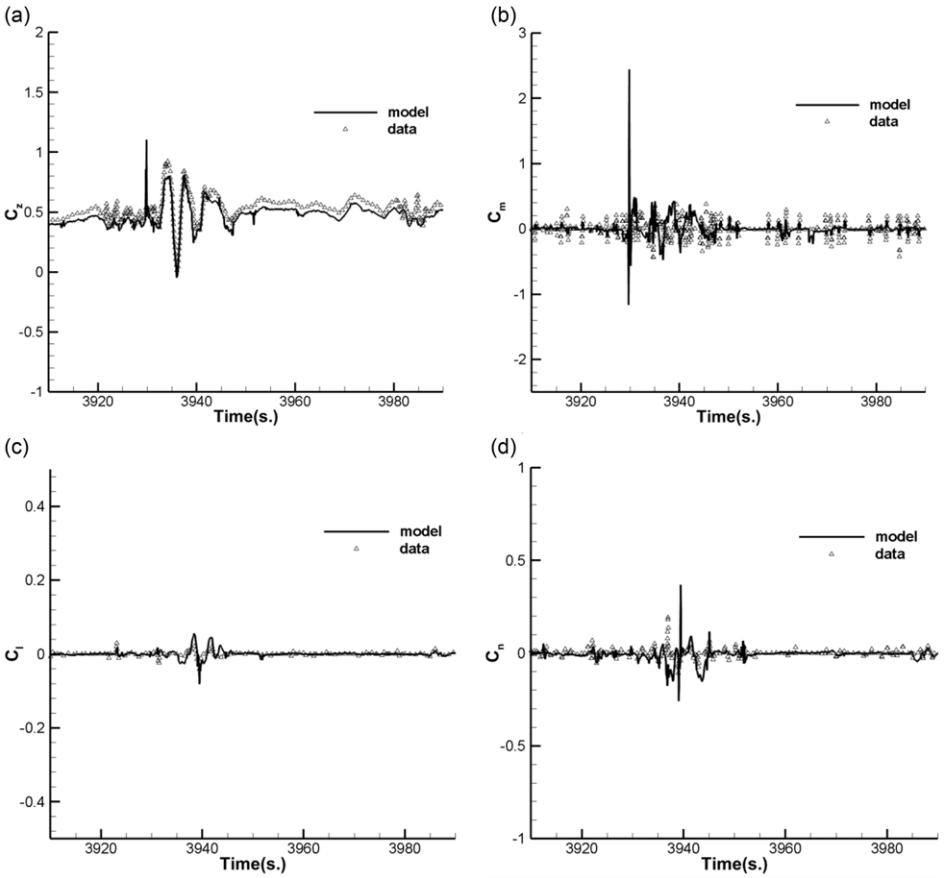

Figure 3. *Comparisons of model-predicted results with modeling input data for Aircraft A.*

The comparisons of model-predicted results with modeling input data for Aircraft A and Aircraft B are shown in Figs. 3 and 4, respectively. Vertical force C_z, pitching moment C_m, rolling moment C_l, and yawing moment C_n. The predicted data of C_z-data by the final models have good match with the input data before the modeling, as shown in Figs. 3(a) and 4(a). The C_m-data in Figs. 3(b) and 4(b) scattering is most likely caused by turbulence-induced buffeting on the structure, in particular on the horizontal tail. The C_l-data in Fig. 3(c) has acceptable comparison and Fig. 4(c) has good match with the input data before the modeling. The C_n-data in Figs. 3(d) and 4(d) have acceptable comparisons with the input data before the modeling. The predicted data by the final models have good match with the input data before the modeling. Once the aerodynamic models are set up, one can calculate all necessary derivatives to analyse the stability.

https://doi.org/10.1017/aer.2024.98 Published online by Cambridge University Press

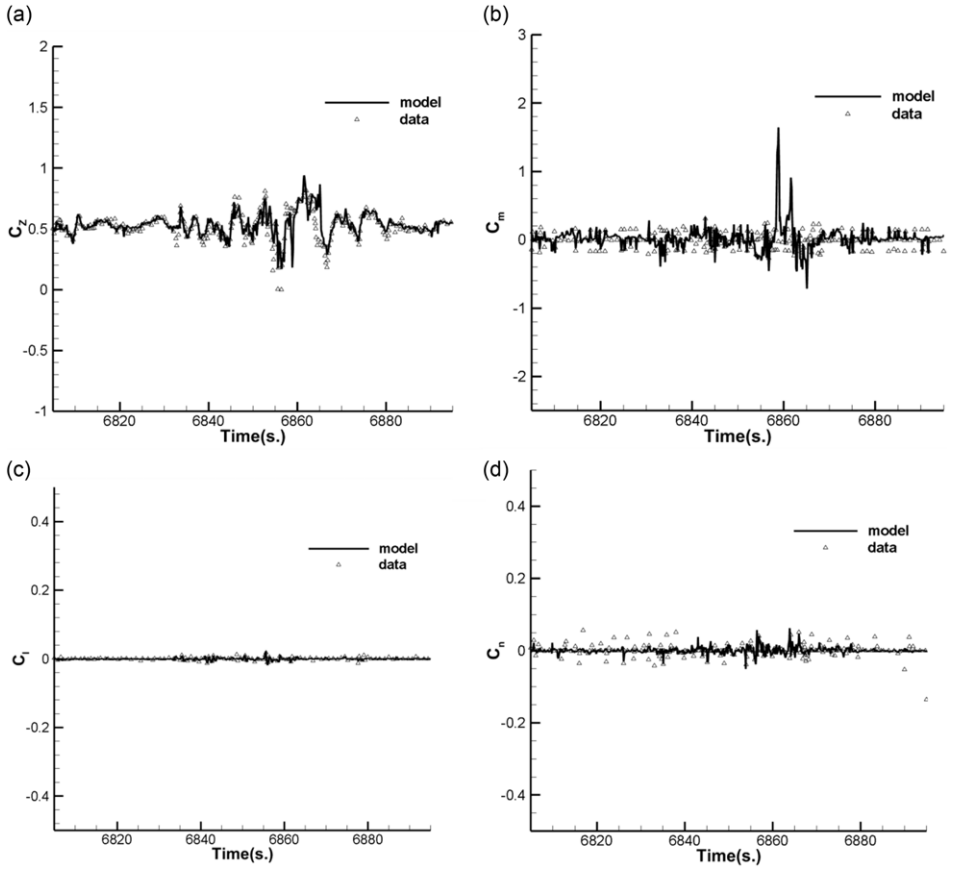

Figure 4. *Comparisons of model-predicted results with modeling input data for Aircraft B.*

3.3 Flight environment analysis

Aerodynamic situations can reflect the quality of the flight environment. The corresponding flight data of Aircraft A and B are extracted from flight data record (FDR) in time spans $t = 3{,}910$–$3{,}990$s and $t = 6{,}805$–$6{,}895$s, respectively. The changes in nonlinear unsteady behaviour and major flight variables in the flight environment of Aircraft A and B are shown in Table 7. One can select the minimum and maximum values of each flight variable within the time span. The other flight variables use the same method to establish Table 7.

3.3.1 Aerodynamic scenario

(1) Aircraft A

Figure 5 shows the relevant flight data of Aircraft A, when it encountered serious atmospheric turbulence during its cruise. The analysis model was built using data from the flight data over a period of $t = 3{,}898$–$3{,}990$s, during which Aircraft A encountered a serious atmospheric turbulence. Figure 5(a) variations of the normal acceleration a_z over time shows that a_z reaches a maximum of 1.74g at about 3,934s and a minimum of 0.015 g at $t = 3{,}936$s, in which case the passenger is highly likely to be injured due to the rapid change in g value. Figure 5(b) shows that the maximum angle-of-attack α when encountering atmospheric turbulence is about 6.6 deg.

Figure 5(c) shows the variations of altitude h changing with time when encountering atmospheric turbulence. It shows that the highest vertical descent height of the aircraft in the process of fluctuating movement when encountering atmospheric turbulence is $t = 3{,}922$–$3{,}934$s, and the altitude reaches

https://doi.org/10.1017/aer.2024.98 Published online by Cambridge University Press

Table 7. *The changes in nonlinear unsteady behaviour and major flight variables in the flight environment*

Flight variable	Aircraft A3,910∼3,990 s	Aircraft B6,805∼6895 s
Vertical acceleration a_z (g)	+1.74∼ +0.02	+1.67∼ −0.75
Angle-of-attack α (deg)	+6.8∼ −5.5	+6.2∼ −5.9
Mach number (M)	0.81∼0.77	0.88∼0.83
Largest drop-off height (m)	67.1	57.8
Wind speed (m/s)	+262.6∼ +223.7	+79.8 ∼ +40.9
Wind direction (deg)	+281.0 ∼ +270.3	+155.0 ∼ +92.0
Drift angle (deg)	+10.0∼ +7.4	+5.0 ∼ 0.0

67.056m. Figure 5(d) shows the Mach number M change over time, with the Mach number dropping from 0.8092 to 0.7721 when Aircraft A encountered turbulence.

(2) Aircraft B

Figure 6 shows the relevant flight data of Aircraft B when it encountered serious atmospheric turbulence during cruise. The sampling period of the research data was t = 6,805–6,895s. Figure 6(a) shows that the normal acceleration a_z reaches a peak of 1.67 g with t about 6,853s, and drops to a minimum of 0g at t about 6,856s. Figure 6(b) shows that the change in the angle-of-attack α is roughly in sync with the change in a_z, reaching a maximum of about 6 degrees, which is already significantly above the cruising phase standard value. Figure 6(c) shows that when the height h is the highest (t = 6,853s), the maximum instantaneous height drop is about 28.65m. Figure 6(d) shows that the Mach number M also drops from the stable value of 0.86 to about 0.844 at the same time.

It can be expected that the dynamic aerodynamic effect is very large in the case of instantaneous changes of α, h, and M in transonic flight. Since the angle-of-attack α of aircraft A and B in transonic flight reaches about 6.0 degrees, the effect of compression effect is very large. The maximum a_z value of flight A is larger than that of flight B, and the change of altitude and angle-of-attack of flight A is also larger than that of flight B.

3.3.2 Aircraft responses in flight operations

(1) Aircraft A

Figure 7 presents the variations of dynamic characteristics and control variables for Aircraft A The changes of α and sideslip angle (β) including turbulence effects are shown in Fig. 7(a). The variation ranges of α are 6.5 deg. to −6 deg. in turbulence encounter; the time history of β values are about ±2 degrees during the period t = 3,930–3,950s, as indicated in Fig. 7(a). The time history of θ and ϕ is shown in Fig. 7(b). The θ does not vary as much as α, but the highest value reaches 5.1 deg. The variations of ϕ is large with the variations −18–10 deg. during the turbulence encounter. The magnitudes of q and p are shown in Fig. 7(c); the variation of roll rate p is large from - 9 to 20 deg/s; the variation of p is much larger than that of q.

(2) Aircraft B

Figure 8 shows the dynamic characteristics of Aircraft B and changes in the control variables. The variation of angle-of-attack α and sideslip β is shown in Fig. 8(a). The variation of α is about 6 deg to −6 deg, and the variation of β is small about 0 deg. In Fig. 8(b), the variations in θ and ϕ amplitude appear to be the same but differ in magnitude, especially with large variations in ϕ amplitude with −12 to 12 deg; θ changes only slightly, reaching only about 7.5 deg. The magnitude of pitch rate q and roll rate p are shown in Fig. 8(c). The variation of roll rate p is large from - 5 to 10 deg/s. The change of p is greater than that of q. The yaw rate r is not shown in the figure because the value is much smaller than p and q.

https://doi.org/10.1017/aer.2024.98 Published online by Cambridge University Press

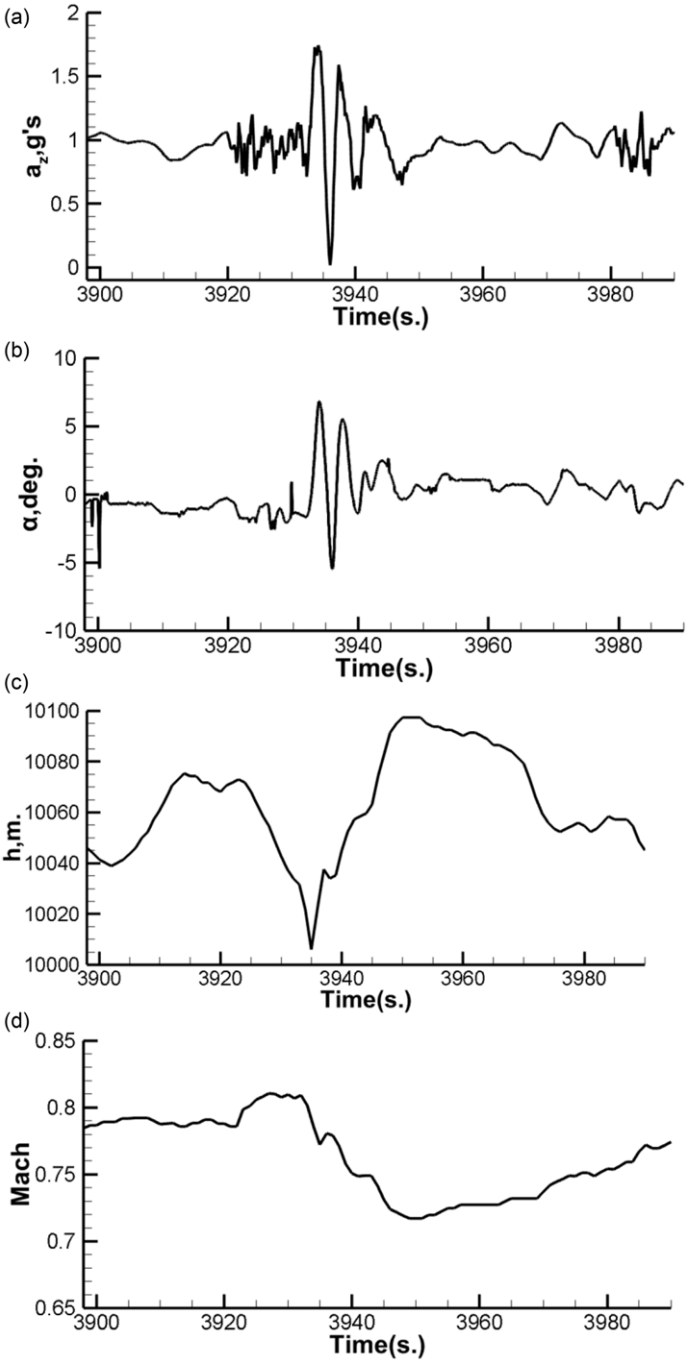

Figure 5. *Aerodynamic scenario of Aircraft A encountering atmospheric turbulence.*

3.4 Eigenvalue analysis of nonlinear unsteady behaviour

In this article, the longitudinal and lateral-directional motion modes are analysed through the digital flight simulation based on the decoupled dynamic equations of motion. The eigenvalue equation is expressed and solved in polynomial form. The longitudinal motion has short-period and phugoid

https://doi.org/10.1017/aer.2024.98 Published online by Cambridge University Press

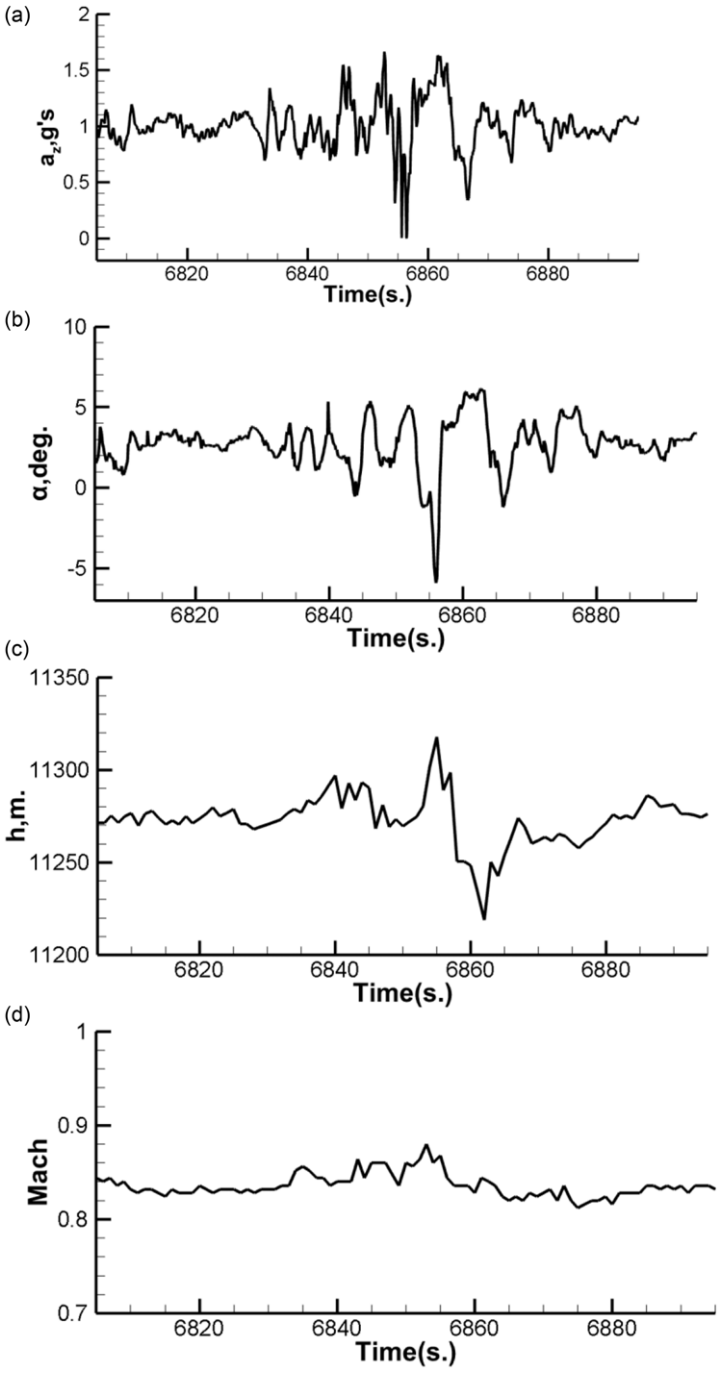

Figure 6. *Aerodynamic scenario of Aircraft B encountering atmospheric turbulence.*

(long-period) modes; the lateral-directional motion has Dutch-roll, spiral and roll modes. The analysis of both longitudinal and lateral-directional motion modes is based on damping ratio and undamped natural frequency [12]. The roots of the complex conjugate are as follows:

$$\lambda_{r,i} = -\zeta\omega_n \pm i\omega_n\sqrt{1-\zeta^2} \tag{18}$$

https://doi.org/10.1017/aer.2024.98 Published online by Cambridge University Press

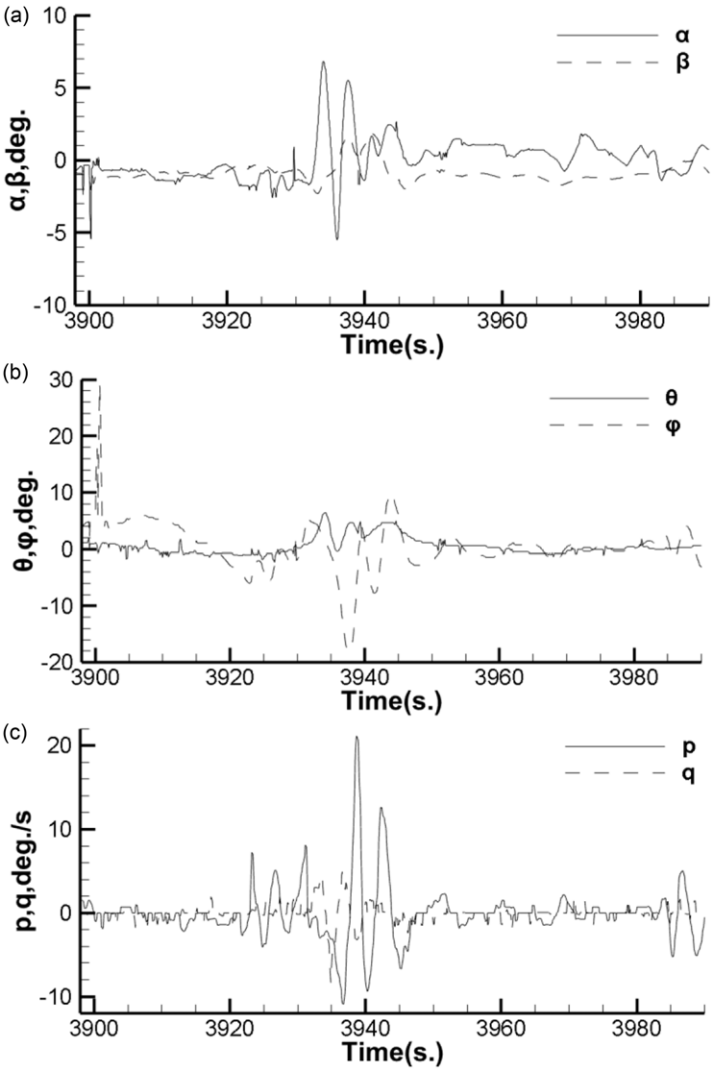

Figure 7. *Aircraft responses in flight operations for Aircraft A encountering atmospheric turbulence.*

where $-\zeta\omega_n$ is real part (i.e. in-phase) and $\pm i\omega_n\sqrt{1-\zeta^2}$are imaginary (i.e. out-of-phase) parts. λ_r and λ_i represent eigenvalues of real and imaginary parts, respectively. If λ_r is positive, the positive real part of the eigenvalues is to indicate unstable motion of the related modes; if it is negative, the motion is stable.

3.4.1 Eigenvalue analysis of motion modes for Aircraft A

(1) Longitudinal motion modes for Aircraft A

Figure 9 is the longitudinal eigenvalue of Aircraft A. Figure 9(a) and (b) are eigenvalue of short-period and phugoid (long-period) modes, respectively. In Fig. 9(a), the real part eigenvalue is positive, which is expressed as dynamic unstable. Figure 9(b) is the eigenvalues of the real part and imaginary part of the long period mode in the longitudinal motion. The real part eigenvalues in Fig. 9(b) are negative in most of the time, except in the period of 3,930.4–3,930.8 and 3,934.9–3,935.5s, which are positive. Their size change type is similar to the continuous mountain vein with peak in the negative direction. The imaginary part eigenvalues in Fig. 9(b) are mostly 0 from beginning to end.

https://doi.org/10.1017/aer.2024.98 Published online by Cambridge University Press

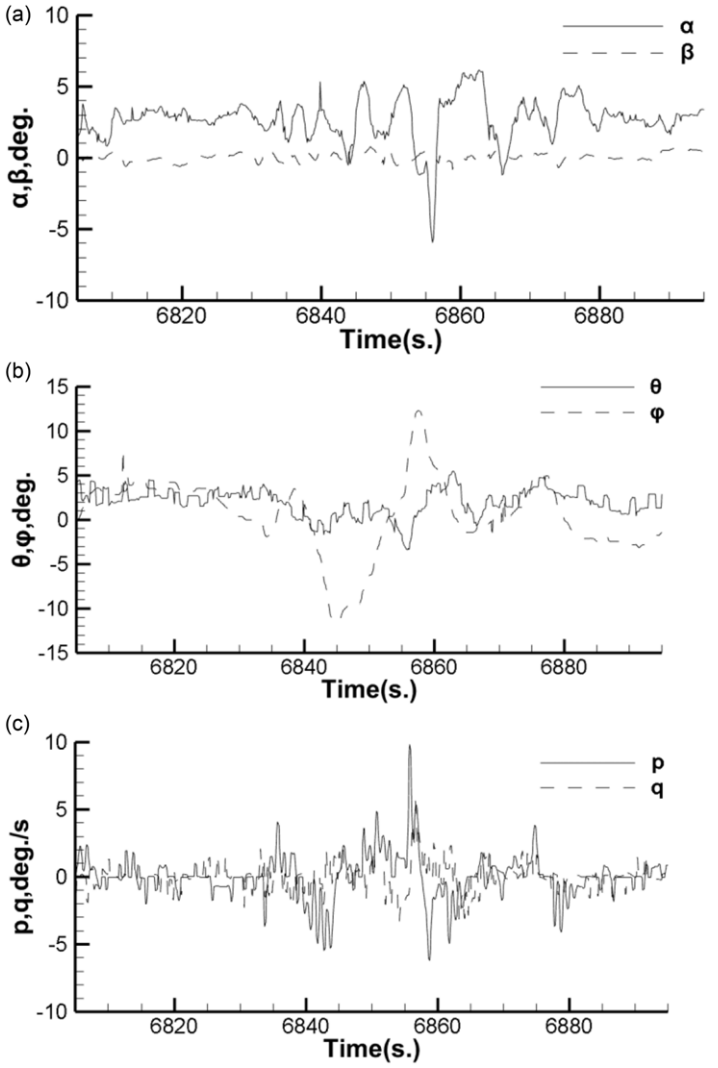

Figure 8. *Aircraft responses in flight operations for Aircraft B encountering atmospheric turbulence.*

(2) Lateral-directional motion modes for Aircraft A

Figure 10 is the lateral-directional eigenvalue for Aircraft A. Figure 10(a), (b), and (c) are eigenvalues of Dutch-roll, spiral and roll modes, respectively. It can be seen from Fig. 10(a) that the first half of the time shows a relatively dynamic unstable situation. Figure 10(b) is the eigenvalue of the spiral mode. In the figure, the real eigenvalue is positive in most of the time, and only a few small parts are negative. Figure 10(c) is the eigenvalues of the roll mode, and the eigenvalues of the real part in Fig. 10(c) are negative.

3.4.2 Eigenvalue analysis of motion modes for Aircraft B

(1) Longitudinal motion modes for Aircraft B

Figure 11 is the longitudinal eigenvalue of aircraft B. Figure 11(a) and (b) are eigenvalue of short-period and phugoid (long-period) modes, respectively. In Fig. 11(a), the eigenvalues of most real parts are negative, except at 6,833.5, 6,856.7 and 6,874.9s. The fluctuation is not much different, and the

https://doi.org/10.1017/aer.2024.98 Published online by Cambridge University Press

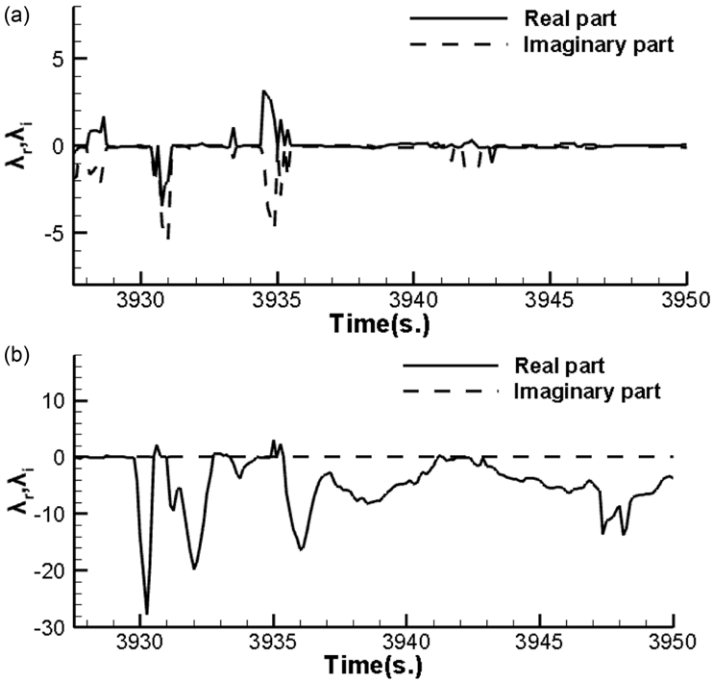

Figure 9. *Eigenvalue analysis of longitudinal motion modes for Aircraft A.*

frequency is more to compared with the short-period mode of aircraft A. The amplitude of eigenvalue fluctuation of the real part in Fig. 11(a) is slightly smaller than that of the imaginary part; the eigenvalue of the imaginary part in Fig. 11(a) fluctuates slightly. Figure 11(b) shows the eigenvalues of the long-period mode in the longitudinal motion, in which the real eigenvalues show a relatively dense peak state during the whole period.

(2) Lateral-directional motion modes for Aircraft B

Figures 12(a)–(c) are the lateral-directional eigenvalue for aircraft B. Figure 12(a), (b), and (c) are eigenvalues of Dutch-roll, spiral and roll modes, respectively. During the whole period, the real and imaginary eigenvalues fluctuated intensively in Fig. 12(a), and the real eigenvalues reached the lowest value at 6,844.2s. The eigenvalue fluctuations are more intensive and slightly larger to compare with the Dutch-roll mode of aircraft A. The real part eigenvalue fluctuates greatly on the whole in Fig. 12(b). Most of the time, it is positive and fluctuates frequently. It reaches the highest value at about 6,845.1s, showing a mountain like peak. The most of the real eigenvalues in Fig. 12(c) are negative, with large fluctuations, reaching the lowest value around 6,856.2s. On the whole, most of the real eigenvalues are negative, which is relatively stable.

Based on the comprehensive analysis of the above two aircraft, the tentative conclusion is as follow:

(1) Assessment of nonlinear unsteady behaviour for longitudinal motion:

The short-period mode is dynamic unstable and long period mode is stable for Aircraft A and Aircraft B.

(2) Assessment of nonlinear unsteady behaviour for lateral-directional motion:

The Dutch-roll mode is dynamic unstable; the spiral mode is dynamic unstable in most of the time; the roll mode is stable for Aircraft A and Aircraft B. The movement mechanism of spiral mode in further investigation is essential.

https://doi.org/10.1017/aer.2024.98 Published online by Cambridge University Press

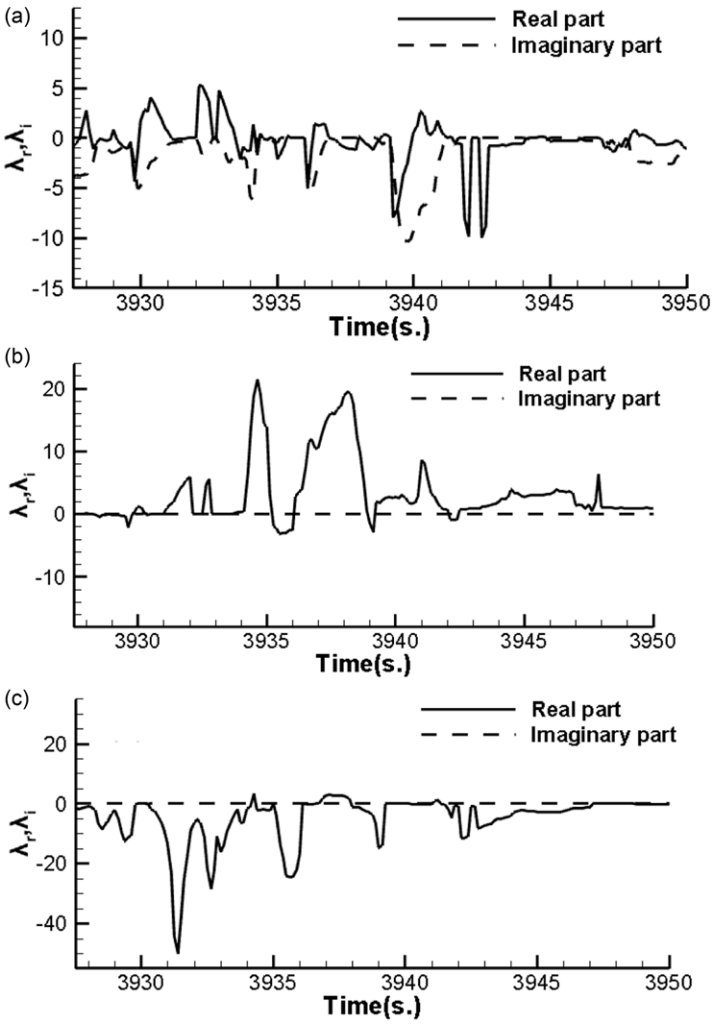

Figure 10. *Eigenvalue analysis of lateral-directional motion modes for Aircraft A.*

(3) Although the changes of the main flight variables in aerodynamic scenarios and flight environments are not the same, the profiles of nonlinear unsteady behaviour for longitudinal and lateral-directional motions are similar through reliability assessment.

3.5 Analysis of dynamic stability characteristics

The comparative analyses of the nonlinear unsteady behaviour for those two aircraft are similar through reliability assessment. Aircraft A has higher dropped-off altitude during the ups and downs motion between the two, so it is chosen to construct the movement mechanism study.

The main longitudinal and lateral-directional oscillatory derivatives of Aircraft A are along the flight path to associate with the derivatives of time rate of angle-of-attack ($\dot{\alpha}$) and sideslip angle ($\dot{\beta}$). The main longitudinal and lateral-directional oscillatory derivatives for Aircraft A are presented in Fig. 13. Note the oscillatory derivatives in Fig. 13 are defined as:

https://doi.org/10.1017/aer.2024.98 Published online by Cambridge University Press

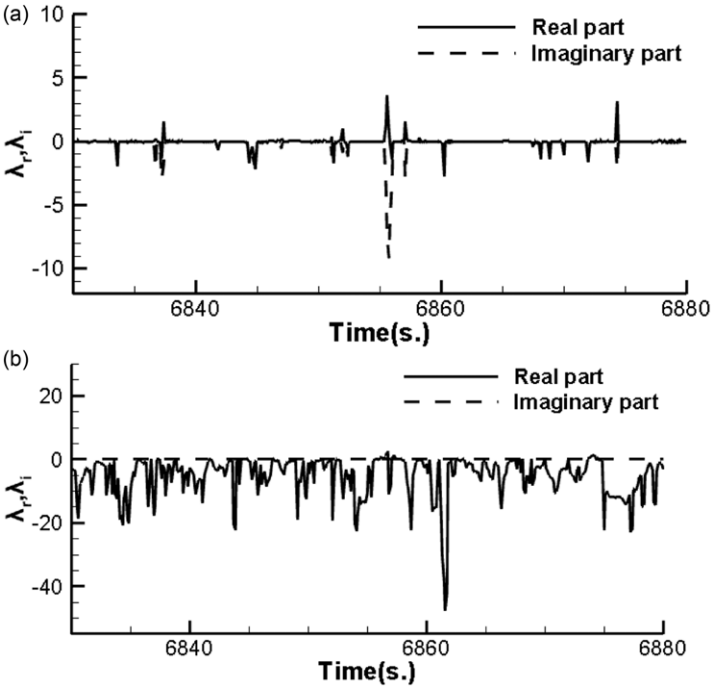

Figure 11. *Eigenvalue analysis of longitudinal motion modes for Aircraft B.*

$$\left(C_{mq}\right)_{osc} = C_{mq} + C_{m\dot{\alpha}} \tag{19}$$

$$\left(C_{zq}\right)_{osc} = C_{zq} + C_{z\dot{\alpha}} \tag{20}$$

Figure 13(a) presents the variations of C_{mq}, $(C_{mq})_{osc}$, and C_{mq} with respect to time. Figure 13(b) presents the variations of $C_{m\dot{\alpha}}$ (i.e. $C_{m\alpha d}$) and $C_{z\dot{\alpha}}$ (i.e. $C_{z\alpha d}$) with respect to time. The damping oscillatory derivatives in Fig. 13(c) are defined as:

$$\left(C_{lp}\right)_{osc} = C_{lp} + C_{l\dot{\beta}} \tag{21}$$

$$(C_{nr})_{osc} = C_{nr} - C_{n\dot{\beta}}\, cosa \tag{22}$$

Equations (19)–(22) show that the oscillatory derivatives are the combination of static damping and dynamic derivatives. The meaning of symbols describes as follows:

(1) For longitudinal aerodynamics

$(C_{mq})_{osc}$: Oscillatory derivative of C_m with respect to q; $(C_{zq})_{osc}$: Oscillatory derivative of C_z with respect to q; C_{mq}: Damping derivative of C_m with respect to q; C_{zq}: Damping derivative of C_z with respect to q; $C_{m\dot{\alpha}}$ (i.e. $C_{m\alpha d}$): Dynamic stability derivative of C_m with respect to $\dot{\alpha}$ and $C_{z\dot{\alpha}}$ (i.e. $C_{z\alpha d}$): Dynamic stability derivative of C_z with respect to $\dot{\alpha}$.

(2) For lateral-directional aerodynamics

$(C_{lp})_{osc}$: Oscillatory derivative of C_l with respect to p; $(C_{nr})_{osc}$: Oscillatory derivative of C_n with respect to r; C_{lp}: Damping derivative of C_l with respect to p; C_{nr}: Damping derivative of C_n with respect to r; $C_{l\dot{\beta}}$ (i.e. C_{lbd}): Dynamic stability derivative of C_l with respect to $\dot{\beta}$ and $C_{n\dot{\beta}}$ (i.e. C_{nbd}): Dynamic stability derivative of C_n with respect to $\dot{\beta}$.

The effectiveness criteria for derivative values are shown in Table 1. When analysing the stability characteristics of an aircraft encountering serious atmosphere turbulence, it is more realistic to use

https://doi.org/10.1017/aer.2024.98 Published online by Cambridge University Press

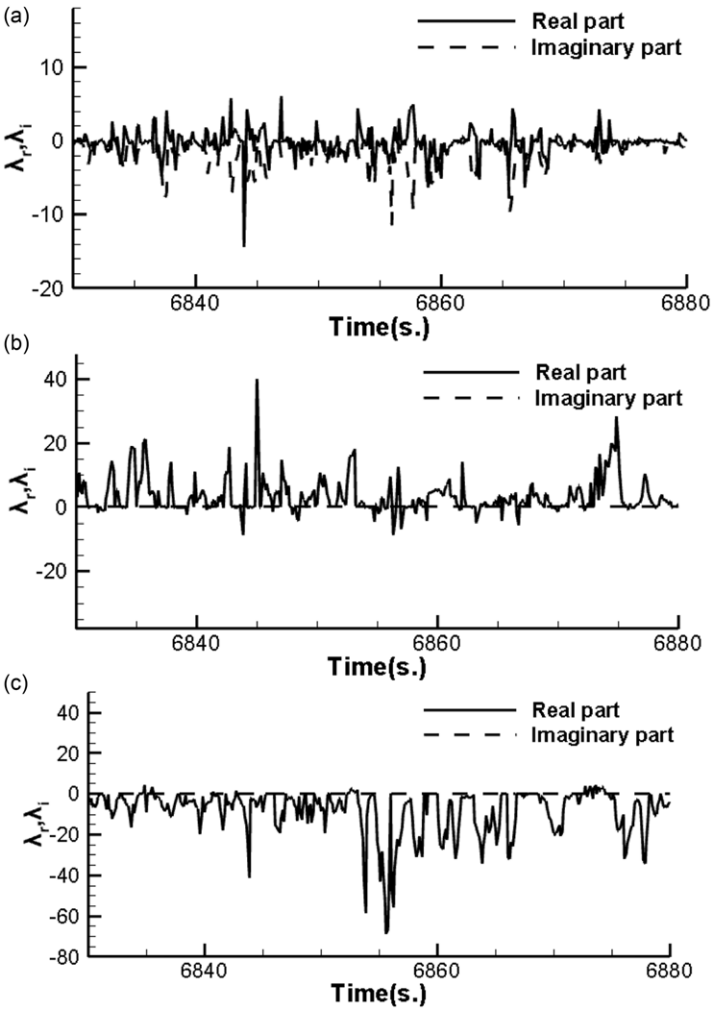

Figure 12. *Eigenvalue analysis of lateral-directional motion modes for Aircraft B.*

damped oscillation derivatives instead of static damping in the analysis of dynamic stability characteristics. Regarding to nonlinear unsteady behaviour, if the behaviour is unstable, the motion will be divergent in oscillatory motions; to be stable, $(C_{zq})_{osc} > 0$, $(C_{mq})_{osc} < 0$, $(C_{lp})_{osc} < 0$, and $(C_{nr})_{osc} < 0$ [17].

The main longitudinal and lateral-directional oscillatory derivatives for Aircraft A are presented in Fig. 13. Figure 13(a) is oscillatory derivatives of C_m and C_z with respect to q. Figure 13(b) is variations of $C_{z\dot{\alpha}}$ and $C_{m\dot{\alpha}}$ with respect to time. Figure 13(c) is main lateral-directional oscillatory derivatives. Figure 13(d) is $C_{l\dot{\beta}}$ and $C_{n\dot{\beta}}$ with respect to time. The values in the period of ups and downs motion have some differences between oscillatory and static damping derivatives in Figs of 13(a) and (c) for Aircraft A due to the effects of the dynamic derivatives (i.e. $\dot{\alpha}$ and $\dot{\beta}$-derivatives). The magnitudes in the period of ups and downs motion have some differences between oscillatory and static damping derivatives in Figure of 13(a) and (c) for Aircraft A due to the effects of the dynamic derivatives.

Figures of 13(b) and (d) show dynamic derivatives of stability for Aircraft A. To be stable, $C_{z\dot{\alpha}} > 0$, $C_{m\dot{\alpha}} < 0$, $C_{l\dot{\beta}} < 0$, and $C_{n\dot{\beta}} > 0$ referred to Table 1. In Fig. 9(a), the eigenvalues of the real part are positive at the beginning, indicating instability because there is not enough damped oscillation in pitching moment $(C_{mq})_{osc} > 0$, as shown in Fig. 13(a). The eigenvalues of the real and imaginary parts of the long-period

https://doi.org/10.1017/aer.2024.98 Published online by Cambridge University Press

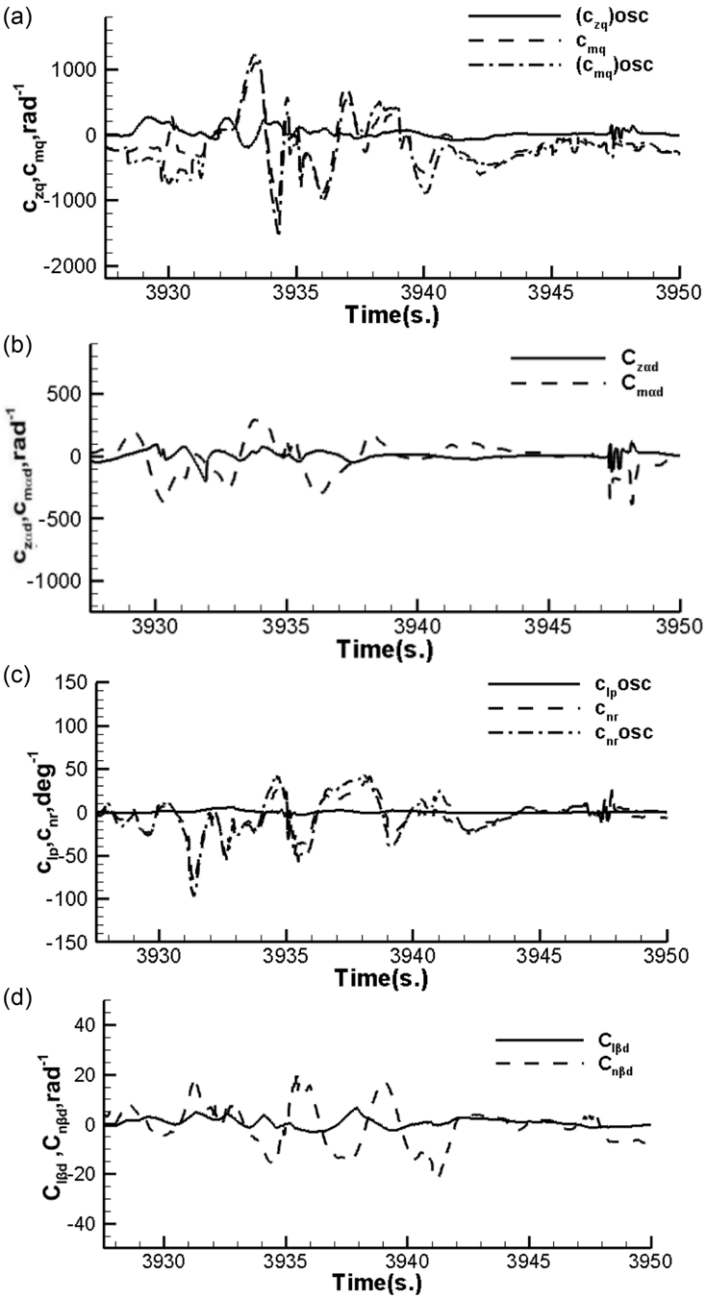

Figure 13. *The main longitudinal and lateral-directional oscillatory derivatives for Aircraft A.*

mode in the longitudinal direction, the eigenvalues of the real part in Fig. 13(b) are negative most of the time, except for a small part of 3,930.4–3,930.8s and 3,934.9–3,935.5s which are positive value, because there is sufficient damped oscillation in pitching moment, as shown in Fig. 13(a).

In Fig. 13(b), the values of $C_{z\dot{\alpha}}$ and $C_{m\dot{\alpha}}$ have significant variations in the period of $t = 3{,}910$–$3{,}990$s, as shown in Fig. 13(b). The most parts of $C_{z\dot{\alpha}}$ are in a nominal negative value. The value of $C_{z\dot{\alpha}}$ represents the virtual mass effect(18) and is particularly large in transonic flow to affect the ups and downs motion.

https://doi.org/10.1017/aer.2024.98 Published online by Cambridge University Press

The magnitudes of $C_{z\dot{\alpha}}$ is in a nominal negative and $C_{m\dot{\alpha}}$ is in a positive in the period of $t = 3{,}928.5$–3,929.5s; then, $C_{z\dot{\alpha}}$ approaches to zero and $C_{m\dot{\alpha}}$ becomes negative value in the period of $t = 3{,}930$–3,931.5s, as shown in Fig. 9(b). The effect of $\dot{\alpha}$-derivative on $(C_{mq})_{osc}$ is to improve the longitudinal motion modes in pitching moment after $t = 3{,}929.5$s in Fig. 13(a) through the magnitude comparisons of $(C_{mq})_{osc}$ with C_{mq}.

From Fig. 10(a) of Dutch-roll mode, it can be seen that the relatively unstable situation is due to the damped oscillation derivative in yawing moment is not enough $(C_{nr})_{osc} > 0$ as shown in Fig. 10(c). The spiral mode in Fig. 10(b) is dynamic unstable in most of the time due to insufficient damped oscillation in yawing moment, as shown in Fig. 10(c). The roll mode is stable because the value of $(C_{lp})_{\text{osc}}$ is mostly negative and thus has sufficient damped oscillation in rolling moment, as shown in Fig. 10(c). The magnitudes of $C_{l\dot{\beta}}$ are positive and some parts of $C_{n\dot{\beta}}$ are negative with unstable conditions in the period of $t = 3{,}923$–3,955s. The effects of $\dot{\beta}$-derivative on $(C_{lp})_{osc}$ and $(C_{nr})_{osc}$ are to cause the directional stability more unstable in Fig. 10(c) through the magnitude comparisons of $(C_{lp})_{osc}$ and $(C_{nr})_{osc}$ with C_{lp} and C_{nr}. It implies that the effects of $\dot{\beta}$-derivatives of $C_{l\dot{\beta}}$ and $C_{n\dot{\beta}}$ in Fig. 10(d) are to cause the spiral mode more unstable.

Based on the analysis of dynamic stability characteristics for Aircraft A, the tentative conclusion is as follow:

The effect of $\dot{\alpha}$-derivative on $(C_{mq})_{osc}$ is to improve the stability in pitch; the effects of $\dot{\beta}$-derivative on $(C_{lp})_{osc}$ and $(C_{nr})_{osc}$ are to cause the lateral-directional stability more unstable. It is especially important for the movement mechanism of the spiral mode.

Regarding to nonlinear unsteady behaviour, if the behaviour is unstable, the motion will be divergent in oscillatory motions; to be stable, $(C_{zq})_{osc} > 0$, $(C_{mq})_{osc} < 0$, $(C_{lp})_{osc} < 0$, and $(C_{nr})_{osc} < 0$ [17].

3.6 Influence of crosswind on loss of control

Wind direction in the QAR or FDR is based on cardinal direction of navigation. It refers to the horizontal angle between the clockwise direction and the target direction from the true north direction of a certain point. The angle between heading and track is known as the drift angle [19]. The crosswind component is computed by multiplying the wind speed by the sine of drift angle. For example, a 10-knot wind coming at 45 degrees of drift angle will have a crosswind component of 10 knots × sin (45°) or about 7.07 knots. If the magnitude of drift angles is large and with variations, the pilots should be educated that the varying crosswind encounter will occur [3].

The flight data of Aircraft A is extracted from FDR in time spans $t = 3{,}910 \sim 3{,}990$s. Figure 14 is rolling motion in crosswind and the corresponding to rolling control for Aircraft A. One takes the time spans $t = 3{,}927$–3,950sec in Fig. 14 for the purpose to study the crosswind before the ups and downs motion. Figure 14(a) is both horizontal wind shear (tailwind) and crosswind. The rolling motion in crosswind and the corresponding to rolling control for Aircraft A are presented in Figures of 14(b) and (c). The roll control power derivative is presented in Fig. 14(d).

Aircraft A is subjected to crosswind with considerable magnitude before the ups and downs motion; the magnitude of drift angles is in the range of $+10.0 \sim +7.4$, which is larger than usual. It is well-known that varying crosswind, would induce rolling motion [3]. The values of roll angles (ϕ) are changed from positive to negative ($t = 3{,}932$–3,942s.) and ϕ reaches -19 deg. at $t = 3{,}939$s in Fig. 14(b), when the crosswind is abruptly increased. In Fig. 14(c), ϕ changes rapidly in the negative value before $t = 3{,}932$s; after the aileron angle (δ_a) becomes more and more positive, reaching 12 degrees at $t = 3{,}939$s. Look at it from a different side, the opposite change occurs around $t = 3{,}935$s. The results show that the corresponding aileron input value does not control it effectively. The roll control power derivative should be positive in the validity criteria. In up-and-down motion, some values of $C_{l\delta a}$ are negative, as shown in Fig. 14(d).

The large variations of roll angles (ϕ) obviously are induced by the influenced of crosswind, the corresponding aileron angle will not be effective to control the roll motion. It implies the large variations are due to the effects of-derivatives of $C_{l\dot{\beta}}$ and $C_{n\dot{\beta}}$. It is the reason why that the spiral mode is dynamic

https://doi.org/10.1017/aer.2024.98 Published online by Cambridge University Press

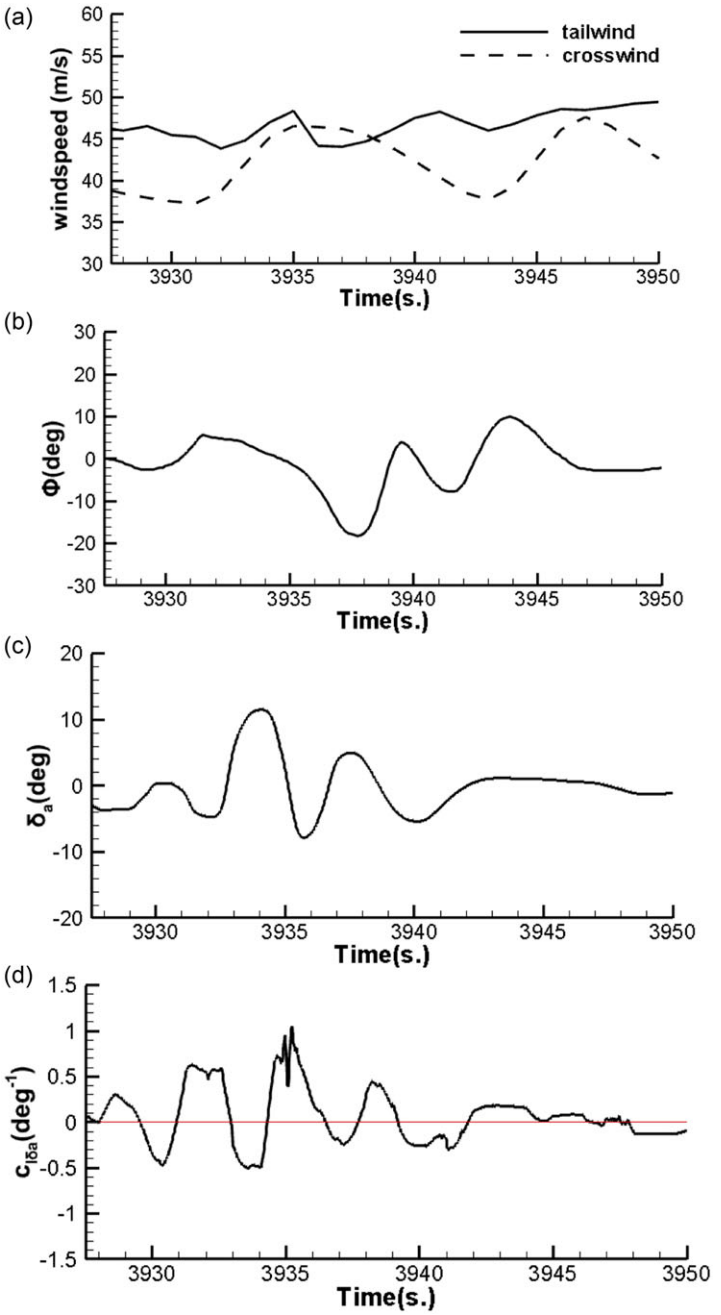

Figure 14. *Rolling motion in crosswind and the corresponding to rolling control for Aircraft A.*

unstable in most of the time. The most loss of control problems happen due to the corresponding control surface angle cannot be effective to control the required flight motion. It is clear that the effects of crosswind cause large changes in the roll angle (ϕ). The corresponding aileron angle will not effectively control the roll motion. Most loss of control problems occur because the corresponding control surface angles are not effective to control the desired flight motion.

https://doi.org/10.1017/aer.2024.98 Published online by Cambridge University Press

3.7 Loss of control prevention in flight motion

The atmosphere turbulence in cruise flight at high altitude is difficult to detect and not easy to predict, but this kind turbulence on the flight route with a certain local area can be specified as a suspected turbulence area. If the drift angle is large in the suspected turbulence area, large crosswind may approach. The varying crosswind will induce rolling motion. The corresponding aileron angle will not be effective to control the roll motion. Most loss of control problems occur because the corresponding control surface angles are not effective for controlling the desired flight motion. Therefore, the rapidly changes of angles of attack (α), flight altitude and Mach number during the ups and downs motion obviously are caused by the aircraft response to the turbulence.

The numerical results and discussions of application to prevent the loss of control are described as follows:

(1) A large drift angle indicated by the instrument is equivalent to an indication that the aircraft will suffer a large crosswind. The crosswind before the turbulence encounter will easily induces rolling motion and then initiates the abrupt ups and downs motion during the turbulence encounter.

(2) The roll rate will increase the oscillatory rolling motion, if the rolling damping is insufficient. The drop-off altitude will be enlarged by the oscillatory rolling motion during the abrupt ups and downs motion.

(3) If the drift angle is large, to remove the autopilot of yaw control first and to stabilise the rudder by the pedal. When passing through the atmosphere turbulence area, the pilots do not need to amend the heading angle urgently.

(4) To provide the mitigation concepts and formulate preventive actions, the situation awareness for the operational pilot before and during severe atmospheric turbulence encounter is consolidated in the present article.

In the future research, one can consider to have more issues of other types of aircraft. It is expected to provide a valuable lecture for international training courses for IATA – Loss of Control In-flight (LOC-I) programme after this paper being published.

4.0 Concluding remarks

The main objective of this article was to present the nonlinear unsteady behaviour for two jet commercial transport aircraft response to serious atmosphere turbulence and to provide the appropriate mitigation concepts for pilots in the pilot training course of the IATA – Loss of Control In-flight (LOC-I) programme. In this article, the eigenvalues of the motion modes for two commercial jet transport aircraft were analysed through digital flight simulation. The digital flight simulation was based on the decoupled dynamic equation of motion. Regarding to the flight simulation in six-DOF, the unstable situations were easily judged by the positive real part of the eigenvalues during abrupt ups and downs motion. I was found that two aircraft of different types and sizes, despite the fact that their aerodynamic scenes and flight environments were not identical, actually had the similar eigenvalues of the motion mode profiles. The effect of $\dot{\alpha}$-derivative was to improve the stability in pitch; the effects of $\dot{\beta}$-derivative were to induce the lateral-directional stability more unstable; it could be clearly shown by the spiral mode. When upstream of jet transport aircraft had crosswind before the turbulence encounter, which would easily induce the rolling motion, and then, induced momentary up and down motions during the turbulence encounter. The magnitude and direction of crosswinds encountered in the flight path could be judged by the drift angle. The alertness of pilots to the changes in the drift angle before and during serious atmospheric turbulence would be the task of further research in the future. The situation awareness responses to the induced mutation of nonlinear unsteady behaviour on the pilot's operations to avoid

https://doi.org/10.1017/aer.2024.98 Published online by Cambridge University Press

loss of control would be a valuable lecture of training course for the IATA - Loss of Control In-flight (LOC-I) programme.

Acknowledgements. This research project is sponsored by the grant of 1KJA460001 from Major Basic Research Project of Natural Science Foundation of Jiangsu Higher Education, the grant of BA2021036 from Special Fund of Jiangsu Province for the Transformation of Scientific and Technological Achievements, and Qinglan Project of Jiangsu Province of China.

Data availability statement. Some or all data, models or code that support the findings of this study are available from the corresponding author upon reasonable request.

References

[1] Storer, L.N., Williams, P.D. and Joshi, M. Global response of clear-air turbulence to climate change, *Geo Res. Lett.*, 2017, **44**, (19), pp 9,976–9,984. doi: 10.1002/2017GL074618
[2] Wang, Y., Chang, R.C. and Jiang, W. Assessment of flight dynamic and static aeroelastic behaviors for jet transport aircraft subjected to instantaneous high g-loads, *Aircraft Eng. Aerospace Technol.*, 2022, **94**, (4), pp 576–589. doi: 10.1108/AEAT-01-2021-0022
[3] Jiang, W., Chang, R.C., Yang, N. and Ding, M. Movement mechanisms for transport aircraft during severe clear-air turbulence encounter, *Aeronaut. J.*, pp 1–25. doi: https://doi.org/10.1017/aer.2022.77
[4] Chang, R.C., Wang, Y. and Jiang, W. Flight control strategy for jet transport in severe clear-air turbulence based on flight data mining, *Aeronaut. J.*, 2023, **1**, (28). doi: 10.1017/aer.2022.52
[5] Dang, Q.V., Vermeiren, L., Dequidt, A. and Dambrine, M. Robust stabilizing controller design for Takagi Sugeno fuzzy descriptor systems under state constraints and actuator saturation, *Fuzzy Sets Syst.*, 2017, **329**, (1), pp 77–90.
[6] IATA, Loss of Control In-Flight Accident Analysis Report. Montreal, Quebec CANADA, Int Air Tran Ass, 2015, LOC-I (flightsafety.org).
[7] Yang, M.H., Ho, C.S., Lan, C.E. and Hsiao, F.B. Longitudinal handling quality analysis of a civil transport aircraft encountering turbulence, *J. Aircraft*, 2010, **47,** (1), pp 32–40.
[8] Han, J., Kamber, M. and Pei, J. *Data Mining: Concepts and Techniques, 3rd ed,* Morgan Kaufmann Publishers, 2013, USA.
[9] Chang, R.C., Lv, Y., Shi, S. and Chen, N. Irregular deviation of flight control surface monitoring for jet transport aircraft, *Aircraft Eng. Aerospace Technol.*, 2022, **94**, (4), pp 633–645. doi: 10.1108/AEAT-04-2021-0121
[10] Jiang, W., Chang, R.C., Yang, N. and Mingwei Ding, M., An investigation of sudden plunging motion mechanisms for transport aircraft during severe clear-air turbulence encounter, *J. Aerospace Eng.*, 2023, **36**, (3). https://doi.org/10.1061/JAEEEZ.ASENG-4493
[11] Lan, C.E. and Chang, R.C. Unsteady aerodynamic effects in landing operation of transport aircraft and controllability with fuzzy-logic dynamic inversion, *Aerospace Sci. Technol.*, 2018, **78**, pp 354–363.
[12] Chang R.C., Ye, C.E., Lan, C.E. and Guan, W.L. Flying qualities for a twin-jet transport in severe atmospheric turbulence, *J. Aircraft*, 2009, **46**, (5), pp 1673–1680.
[13] Chang, R.C. and Tan, S. Examination of dynamic aerodynamic effects for transport aircraft with hazardous weather conditions, *J. Aeronaut. Astronaut. Aviat.*, 2013, **45**, (1), pp 51–62.
[14] Roskam, J. *Airplane Flight Dynamics and Automatic Flight Controls*, DAR Corporation, 2018, Lawrence, Kansas.
[15] Hovanessian, S.A. and Pipes, L.A. *Digital Computer Methods in Engineering*, McGraw-Hill, 1969.
[16] DARcorporation, *Aircraft Design Program, Advanced Aircraft Analysis*, DARcorporation, 2018, Lawrence, Kansas.
[17] Chang, R.C., Ye, C.E., Lan, C.E. and Guan, W.L. Stability characteristics for transport aircraft response to clear-air turbulence, *J. Aerospace Eng.*, 2010, **23,** (3), pp 197–204.
[18] Sheu, D. and Lan, C.E. Estimation of turbulent vertical velocity from nonlinear simulations of aircraft response, *J. Aircraft*, 2011, **48**, (2), pp 645–651.
[19] Drift angle | Article about drift angle by The Free Dictionary, available on Web page: April 7, 2024, https://encyclopedia2.thefreedictionary.com/drift+angle

Cite this article: Jiang W., Guo H., Li Z. and Chang R.C. (2025). Nonlinear unsteady behaviour study for jet transport aircraft response to serious atmosphere turbulence. *The Aeronautical Journal*, **129**, 432–456. https://doi.org/10.1017/aer.2024.98